



Cite this: *New J. Chem.*, 2016, 40, 3323

Amphiphilic unsymmetrically substituted porphyrin zinc derivatives: synthesis, aggregation behavior of the self-assembled films and NO₂ sensing properties†

Yanling Wu,^a Pan Ma,^c Shanshan Liu^a and Yanli Chen^{*ab}

Two novel amphiphilic porphyrin derivatives, 5-(benzo-(4-(2-(2-hydroxy)ethoxy)ethoxy))-10,15,20-triphenylporphyrinato zinc complex [ZnT(OC₂H₄OC₂H₄OH)PP] (**1**) and 5-(benzo-(4-(2-(4,10-*N,N*-15-crown-5)ethoxy)))-10,15,20-triphenylporphyrinato zinc complex [ZnT(OC₂H₄NN15C5)PP] (**2**), were designed, synthesized, and characterized by a range of spectroscopic methods. Their electrochemistry was studied by differential pulse voltammetry (DPV). Highly ordered films of **1** and **2** were fabricated by a solution-based quasi-Langmuir–Shäfer (QLS) technique, and were characterized by electronic absorption spectroscopy, IR spectroscopy, X-ray diffraction, atomic force microscopy (AFM) and current–voltage (*I*–*V*) measurements. Experimental results revealed that J-type aggregates are formed in the QLS film of **1** and **2**. The crystallinity and general molecular order in the film of **1** were improved more effectively than in **2** due to its stronger intermolecular interactions. Furthermore, the conductivity of the QLS film of **1** was approximately 1 order of magnitude larger than that of **2**. This indicates a significant effect of peripheral groups on the conducting behavior of porphyrins. In addition, the gas sensing behavior of the QLS films of **1** and **2** toward the electron acceptor gas, NO₂, was investigated at concentrations 200 and 800 ppm, respectively. The sensitivity, stability, and reproducibility follow the order **1** > **2**, revealing the effect of intermolecular interaction, film structure/morphology, and low-lying LUMO energy level on sensing performance. Unexpectedly, a decreased current response towards NO₂ for the QLS films of both **1** and **2** was obtained for the first time, which unambiguously demonstrated the n-type semiconducting nature of **1** and **2**. The present result represents not only the first example of n-type metalloporphyrin-based thin solid films obtained by a solution-based method, but more importantly provides an efficient way to enhance the performance of n-channel organic semiconductors through the combination of molecular design and the film fabrication technique.

Received (in Montpellier, France)
29th October 2015,
Accepted 29th January 2016

DOI: 10.1039/c5nj03021h

www.rsc.org/njc

1 Introduction

As representatives of functional molecular materials with large conjugated electronic molecular structures, metalloporphyrins and their derivatives, due to properties such as great processability, high

thermal and chemical stability and rich substitution chemistry, are one of the most promising candidates for modern opto-electronic devices such as dye-sensitized solar cells, organic light-emitting diodes, field effect transistors, optical recording and gas sensors.^{1–8} For most of the applications, the properties of the molecular devices are closely related to the microstructures of the solid films. Although many strategies have been explored to control the organization of porphyrin-based building blocks into unique microstructures with different morphology such as fibers, wires, channels, giant micelles, two-dimensional sheets, and cages,^{9,10} it is still a challenge for chemists and materials scientists to construct the porphyrin-based nano-assembly into a highly ordered film-structure using a low-cost, solution-based method through the combination of molecular design and programmed supramolecular interactions.

Nowadays, the interest in developing gas detectors having porphyrin derivatives as the chemically sensitive component of

^a Shandong Provincial Key Laboratory of Fluorine Chemistry and Chemical Materials, School of Chemistry and Chemical Engineering, University of Jinan, Jinan 250022, China. E-mail: chm_chenyl@ujn.edu.cn, yanlichen@upc.edu.cn; Tel: +86 (0)531 8973 6150

^b School of Science, China University of Petroleum (East China), Qingdao 266580, China

^c Jinan Academy of Agricultural Sciences, Jinan 250316, China

† Electronic supplementary information (ESI) available: Experimental isotopic patterns for the molecular ions of **1** (A) and **2** (B) shown in the MALDI-TOF mass spectrum. Polarized UV-vis spectra of QLS films of compounds **1**–**2** (A–B). The time-dependent current plots of the QLS films of **1** (A) and **2** (B) exposed to the different concentrations of NO₂ ranging from 800, 400 to 200 ppm in ambient air, respectively. See DOI: 10.1039/c5nj03021h

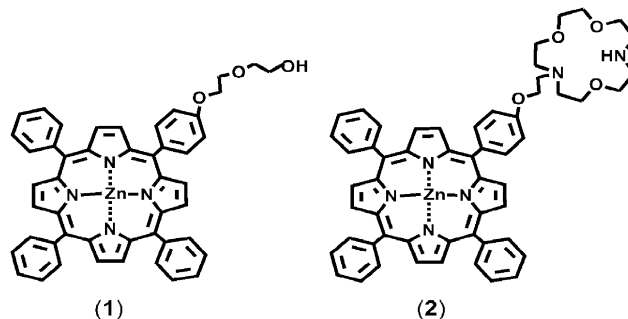
chemical/conductometric transduction systems is steadily increasing, since their electrical properties change upon exposure to oxidizing gases such as NO_2 .^{11–14} It has been found that the synergistic effects of the molecular interactions (such as van der Waals and hydrogen bonding) among porphyrins in the aggregates and the intermolecular porphyrin–analyte coordination interactions determine the sensing performances of the porphyrins.¹⁵ Many efforts have been made to clarify the relationships between the molecular ordering in the film of the porphyrins and the sensing performances. For example, Kerdcharoen *et al.* found that an annealed MgTPP film with improved film-structure exhibited better response to VOCs than a non-annealed MgTPP film.¹⁶ Valli *et al.* reported that the conductivity of the porphyrin compounds attached with electron withdrawing substituents, which exhibit n-type semiconducting behavior, increases in the presence of electron donor gases such as NH_3 and decreases in the presence of electron acceptor gases such as O_2 and NO_x .¹¹ The sensitivity of porphyrins towards analytes significantly improves, when the functionalization on the periphery of the macrocycle or the central metal atom inside the porphyrin core is modified.¹¹

On the other hand, the thin films can be produced by a variety of techniques, such as vacuum sublimation, electron-beam evaporation and simple solution-processing methods. Soluble molecules can be deposited by solution-processing methods, including casting techniques, such as drop casting, spin-coating, or *via* layer-by-layer assembly techniques such as Langmuir–Blodgett (LB: vertical transfer), Langmuir–Shäfer (LS: horizontal transfer) and quasi-Langmuir–Shäfer (QLS) protocols, the surface-assisted self-assembly technique, *etc.* LB, LS and QLS techniques allow one to obtain films with good thickness control and offer the possibility to easily produce multi-layer structured films by applying an external compression force at the air–water interface. In particular, the QLS method developed by Bouvet's group requires no sophisticated set-up with a lower cost relative to LS, which has been employed to obtain the well-organized films of amphiphilic molecules at the air–water interface.^{17–19,28} To gain an insight into the gas-sensing nature of amphiphilic metalloporphyrin molecules, in the present paper, we describe the synthesis and electrochemical properties of two novel amphiphilic porphyrin derivatives, 5-(benzo-(4-(2-(2-hydroxy)ethoxy)ethoxy))-10,15,20-triphenylporphyrinato zinc complex [$\text{ZnT}(\text{OC}_2\text{H}_4\text{OC}_2\text{H}_4\text{OH})\text{PP}$] (**1**) and 5-(benzo-(4-(2-(4,10-*N,N*-15-crown-5)ethoxy))-10,15,20-triphenylporphyrinato zinc complex [$\text{ZnT}(\text{OC}_2\text{H}_4\text{NN15C5})\text{PP}$] (**2**), Scheme 1. Highly ordered films of **1** and **2** were fabricated by a solution-based quasi-Langmuir–Shäfer (QLS) technique. The electrical conductivity of the film of **1** was measured to be approximately 1 order of magnitude larger than that of the film of **2**. The gas sensing behavior of the QLS films of **1** and **2** toward NO_2 was investigated at concentrations 200 and 800 ppm.

2 Results and discussion

2.1 Molecular design, synthesis, and electrochemistry

The 5-(benzo-(4-(2-(2-hydroxy)ethoxy)ethoxy))-10,15,20-triphenylporphyrinato zinc complex [$\text{ZnT}(\text{OC}_2\text{H}_4\text{OC}_2\text{H}_4\text{OH})\text{PP}$] (**1**) was



Scheme 1 Schematic structures of [$\text{ZnT}(\text{OC}_2\text{H}_4\text{OC}_2\text{H}_4\text{OH})\text{PP}$] (**1**) and [$\text{ZnT}(\text{OCH}_2\text{CH}_2\text{NN15C5})\text{PP}$] (**2**).

synthesized according to a recently developed procedure.²⁰ For the purpose of comparative study, the 5-(benzo-(4-(2-(4,10-*N,N*-15-crown-5)ethoxy))-10,15,20-triphenylporphyrinato zinc complex [$\text{ZnT}(\text{OC}_2\text{H}_4\text{NN15C5})\text{PP}$] (**2**) was also prepared following published methods.²⁰

All the newly prepared porphyrinato zinc compounds gave satisfactory test results. The matrix-assisted laser desorption/ionization time-of-flight (MALDI-TOF) spectra of all these compounds showed the molecular ion (M^+) signals with a correct isotopic pattern, as shown in Fig. S1 (ESI[†]). The ^1H NMR spectra of newly prepared porphyrinato zinc compounds **1–2** were recorded in CDCl_3 at room temperature (see ESI[†]).

The electrochemical behavior of the two porphyrinato zinc compounds **1–2** was investigated using differential pulse voltammetry (DPV) in CH_2Cl_2 . These compounds display one one-electron reduction labelled as Red_1 and three one-electron oxidation ($\text{Oxd}_1\text{–Oxd}_3$) within the electrochemical window of CH_2Cl_2 under the present conditions. The half-wave redox potential values *vs.* SCE (standard calomel electrode) are summarized in Table 1. Representative differential pulse voltammograms for **1** and **2** are displayed in Fig. 1. Their highest occupied molecular orbital (HOMO) and lowest unoccupied molecular orbital (LUMO) energy levels were estimated to be about -5.81 and -3.88 eV for **1** and -5.21 and -3.60 eV for **2**, respectively, based on DPV measurements.²¹

2.2 UV-vis absorption spectra

The electronic absorption spectra of the two unsymmetrical porphyrinato zinc derivatives **1** and **2** were recorded in chloroform, Fig. 2 (solid line). As shown in Fig. 2, the compounds **1** and **2** show a characteristic Soret band at *ca.* 420 and 421 nm, respectively. In addition, two satellite Q-bands at 548 and 587 nm are observed for **1** and at 553 and 602 nm for **2**. These observations are in line with the reports for metalloporphyrins.^{22,23} After being fabricated into the QLS film, the UV-vis absorption spectra of **1** and **2** exhibited remarkable red-shifts, when compared to the absorption in solution, from 420, 548, and 587 nm to 437, 561, and 601 nm for **1** and from 421, 553, and 602 nm to 440, 563, and 604 nm for **2**, respectively, Fig. 2 (dashed line). This indicates the formation of J-type molecular packing structure (J aggregation) due to the strong exciton coupling between the neighbouring molecules in the films of **1** and **2**.^{24,25}

Table 1 Half-wave redox potentials of [ZnT(OC₂H₄OC₂H₄OH)PP] (**1**) and [ZnT(OC₂H₄NN15C5)PP] (**2**) (V vs. SCE) in CH₂Cl₂ containing 0.1 mol dm⁻³ [Bu₄N][ClO₄] together with the HOMO and LUMO levels of **1** and **2**

Compound	Red ₁ /V	Oxd ₁ /V	Oxd ₂ /V	Oxd ₃ /V	HOMO/eV ^a	LUMO/eV ^a	ΔE _{1/2} ^o /eV ^b
1	-1.46	0.47	0.77	1.12	-5.81	-3.88	1.93
2	-1.21	0.38	0.67	0.97	-5.21	-3.60	1.59

^a Calculated from the empirical formula of HOMO = -(Oxd₁ + 4.44 eV); LUMO = -(Red₁ + 4.44 eV).²¹ ^b ΔE_{1/2}^o = Oxd₁ - Red₁, the HOMO-LUMO gap of the corresponding molecule.

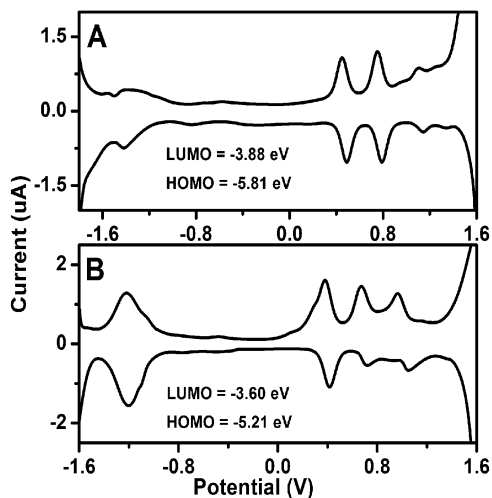


Fig. 1 Differential pulse voltammograms of **1** (A) and **2** (B) in CH₂Cl₂ containing 0.1 M [NBu₄][ClO₄] at a scan rate of 20 mV s⁻¹, respectively.

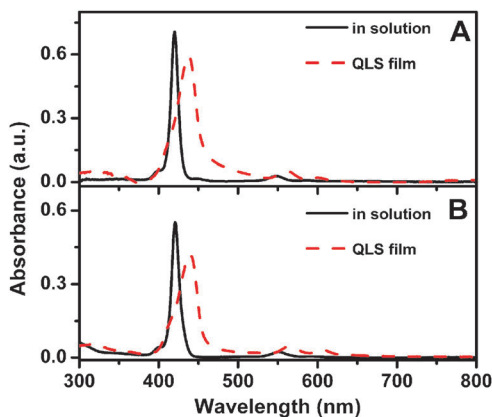


Fig. 2 UV-vis absorption spectra of **1** (A) and **2** (B) in CHCl₃ solution (solid line) and the QLS films (dashed line).

Furthermore, larger red-shifts of absorption bands were achieved in QLS films of **1** compared to **2**, implying an effect of the substituent group incorporated into the *meso*-substituted phenyl group of the porphyrin ring on the intermolecular interaction in solid films. This is also supported by the orientation angle (dihedral angle) revealed for the porphyrin ring with respect to the substrate. As shown in Fig. S2 and Table S1 (ESI[†]),²⁶ the orientation angles of porphyrin rings to the quartz plate surface in the QLS films of [ZnT(OC₂H₄OC₂H₄OH)PP] (**1**)

and [ZnT(OC₂H₄NN15C5)PP] (**2**) are calculated to be 48.7° and 34.5°, respectively, according to polarized UV-vis measurements. This indicates again that molecules of both **1** and **2** take a slipped co-facial stacking mode with an “edge-on” configuration in the QLS films. Note that a larger orientation angle of the porphyrin ring with a relatively large red-shift of absorption bands in the film of **1** resulted from more effective intermolecular interaction in the J aggregates together with the intense intramolecular π-π stacking, which were expected to provide the π electrons with an extensive area for delocalization in the film of **1**. This forms the most basic necessary characteristics for an organic semiconductor with good charge transport ability.^{27,28}

2.3 IR spectra

The IR spectra of [ZnT(OC₂H₄OC₂H₄OH)PP] (**1**) and [ZnT(OC₂H₄NN15C5)PP] (**2**) bulk samples together with their QLS films are compared in Fig. 3. The positions of the peak frequencies in the high-frequency region of 2800–3000 cm⁻¹, which feature the symmetric and asymmetric C–H stretching from CH₂ groups (ν_s(CH₂) and ν_a(CH₂)) in the side chains, provide insight into the intermolecular environment of the alkoxy chains of **1** and **2** in the QLS films relative to the corresponding bulk samples. Previous IR studies have shown that the location of these peaks is a sensitive indicator of the extent of lateral interactions.^{17,29,30} For example, the peak frequencies at 2927 and 2871 cm⁻¹ in the bulk-phase of **1**, which are attributed to the ν_a(CH₂) and ν_s(CH₂) stretching modes from the (O)C–H vibration of the ethoxyglycol side chain, shifted to lower positions at 2925 and 2853 cm⁻¹ in

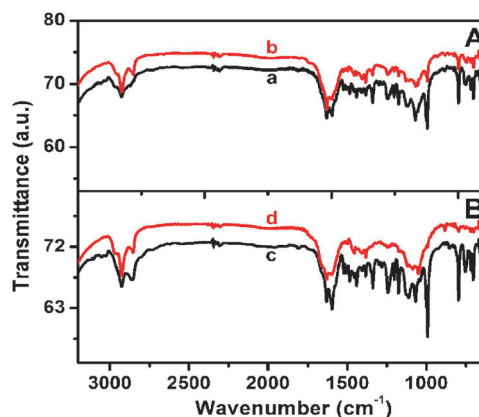


Fig. 3 IR spectra of **1** (A) and **2** (B) in the bulk samples (a and c) and the QLS films (b and d), respectively.

the QLS film of **1**, Fig. 3A. The same phenomena could also be observed for the peak frequencies of **2** from the (O)C–H vibration of the ethoxy side chain with the $\nu_a(\text{CH}_2)$ and $\nu_s(\text{CH}_2)$ modes at 2927 and 2865 cm^{-1} in the bulk-phase and 2925 and 2853 cm^{-1} in the QLS film. A definite trend toward lower peak frequencies of the QLS film compared to the bulk-phase for either **1** or **2** indicated that the side chains are more ordered in the films than in the bulk-phases.^{31,32}

2.4 X-Ray diffraction patterns

The quality of the thin films as well as the preferred molecular orientation was assessed using the out-of-plane (OOP) X-ray diffraction (XRD) technique. Both compounds **1** and **2** deposited on SiO_2 substrates give one distinct diffraction peak in their low angle region, respectively, Fig. 4, indicating that the molecules of either **1** or **2** are uniformly oriented relative to the substrate plane with a layered structure in the films.^{19,33} The OOP XRD of the QLS film of **1** and **2** exhibits the (001) Bragg peak at $2\theta = 7.24^\circ$ and 5.44° , respectively, corresponding to a periodic spacing distance of 1.22 and 1.62 nm. Judging from the geometry-optimized molecular length of **1** and **2** (1.59 and 2.53 nm), tilt angles relative to the substrate of 50.1° and 39.8° are estimated for **1** and **2**, respectively. This corresponds well with the result of polarized UV-vis spectra, indicating again that the molecules of both **1** and **2** take a slipped co-facial stacking mode with an “edge-on” configuration in the QLS films. In addition, the XRD patterns for the QLS films of both **1** and **2** also present one sharp refraction at 0.31 nm, which is attributed to the π - π stacking distance between tetrapyrrole cores of neighboring porphyrin molecules along the direction perpendicular to the tetrapyrrole rings.³⁴ It is worth noting that, in comparison with the film of **2**, the (001) diffraction peak with increased intensity and sharpening in the low-angle region was obtained for the film of **1**, Fig. 4, which indicates the obviously improved molecular ordering and enhanced crystallinity in the film of **1** relative to that of **2**. The better crystallinity in the QLS films of **1** compared to that of **2** can be related to not only improved co-planarity by the unique co-facially stacking structure, but more importantly to the minimization of steric

repulsions by the substituent ethoxyglycol side chain (which results in a highly ordered and denser molecular packing and aligned nature of **1** in the films).

2.5 Morphology of the QLS film

The morphology of the QLS films of **1–2** was also characterized by atomic force microscopy (AFM). The surface of the QLS film of **1** presents a granular structure with uniform grain crystallites, approximately 70 nm in diameter, whereas that of **2** exhibits nanoparticles with an average diameter of *ca.* 60 nm, Fig. 5. The increase in both the grain size and the grain crystallinity would be beneficial to the charge transport in the QLS film of **1** relative to that of **2**.

2.6 *I–V* properties

The porphyrin derivatives with a uniform membrane structure would be promising candidates for applications in electronic devices. To demonstrate the potentials of these QLS films, these films were carefully transferred onto the glass substrate with ITO interdigitated electrodes (IDEs). Fig. 6 shows the current–voltage (*I–V*) characteristics of the porphyrin derivatives of QLS films. The electronic conductivity is calculated to be around $1.5 \times 10^{-2} \text{ S m}^{-1}$ and $2.7 \times 10^{-3} \text{ S m}^{-1}$ respectively. It is noteworthy that the high electrical conductivity (*ca.* 10^{-2} – 10^{-3} S m^{-1}) has also been reported for nanobelts of the amphiphilic perylene-tetracarboxylic diimide derivatives with the typical n-type character by several research groups,^{35,36} which is attributed to

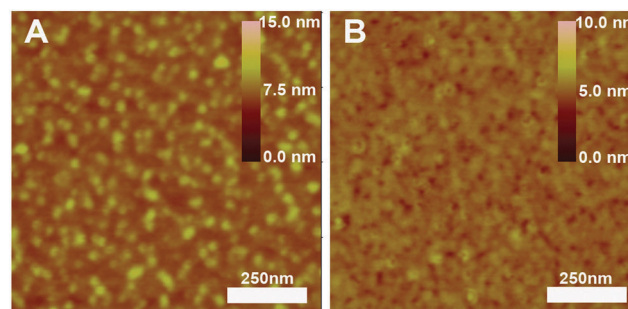


Fig. 5 AFM images of the QLS films of **1** (A) and **2** (B) on the SiO_2 substrates.

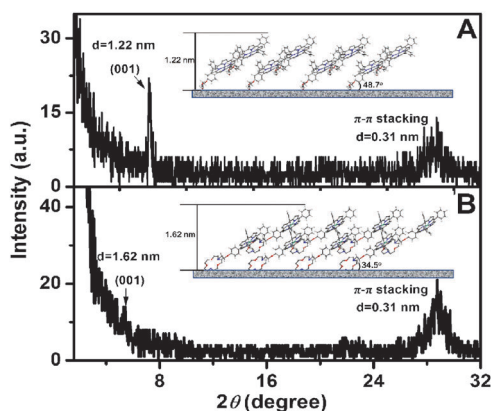


Fig. 4 X-ray patterns for the QLS films of **1** (A) and **2** (B) deposited on SiO_2 substrates. The insets are schematic diagrams of the packing modes of the molecules **1** and **2** in the QLS film, respectively.

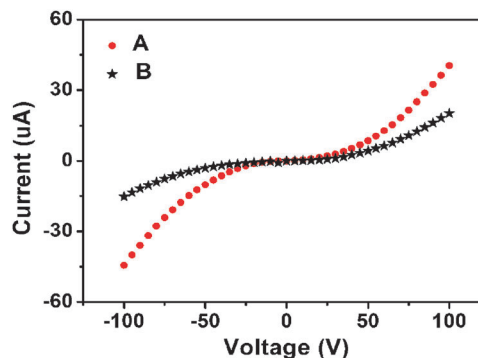


Fig. 6 *I–V* curves measured for the QLS films of **1** (A) and **2** (B) deposited on ITO IDEs/glass substrates, respectively.

ordered one-dimensional π - π stacking (cofacial π -electron delocalization). In the present case, the much higher conductivity in the QLS film of **1** compared to that of **2** might be due to the stronger intermolecular interactions and higher ordered crystalline molecular arrangement in the QLS film of **1**. These films with such high current modulation could be useful for a wide range of electronic and sensor devices.

2.7 Sensor performance measurements

The response of the QLS film-based sensors from **1** and **2** deposited onto the ITO IDEs/glass substrates was determined from the time-dependent current plots when the films were exposed to NO₂ gas in nitrogen at room temperature. As shown in Fig. 7A, when the QLS films of **1** were exposed to 200 and 800 ppm NO₂ (with a duty cycle where the dynamic exposure period is fixed at 4 min and the recovery period at 6 min), respectively, the conductivity decreased during exposure and increased to its initial value during recovery, indicating a good reversibility characteristic in the films. A similar behavior has already been observed in cobalt phthalocyanine³⁷ and bis(phthalocyaninato)holmium.³⁸ A similar response was observed for the film of **2**, but the result is poorer with a slow duty cycle of 7 min/7 min. Since the 5,10,15,20-tetraphenylporphyrin compound as a p-type organic semiconductor has been reported by Checconi and co-workers,³⁹ the n-type sensing response to NO₂ of **1** and **2** unambiguously reveals the significant substituent effect on tuning the nature of porphyrin organic semiconductors. It is well known that, n-type porphyrin-based films are easily oxidized by the electron-accepting gas, NO₂, forming charge-transfer complexes upon analyte (NO₂) binding to these films, which inject holes and decrease film currents.⁴⁰

In order to quantitatively analyze the sensor responses, we define relative response intensity $S = (\Delta I/I_0) \times 100\%$, where I_0 is the baseline current value and $\Delta I = I_g - I_0$; I_g is the current value when the NO₂ gas is switched on. The relative response intensities at 200 and 800 ppm are 74.7% and 86.9% for the film of **1**, and 19.6% and 24.3% for the film of **2**. The higher S value of the film of **1** resulted not only from the better film-quality with stronger molecular interactions among the adjacent molecules in the film of **1**, but more importantly from

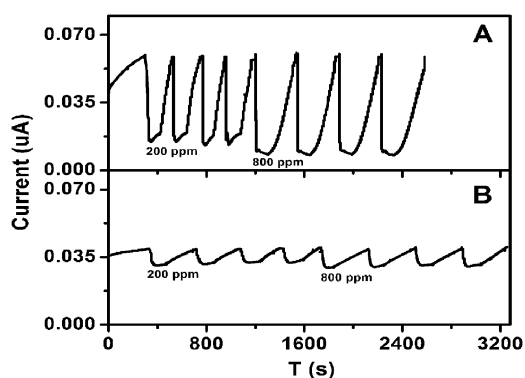


Fig. 7 The time-dependent current plots of the QLS films of **1** (A) and **2** (B) exposed to NO₂ with the concentrations of 200 and 800 ppm for every four cycles, respectively.

the smaller mismatch between the low-lying LUMO energy level of **1** (−3.88 eV) and the work function of the ITO electrode (−4.5 eV)⁴¹ which results in a smaller energy barrier for electron injection. It is worth noting that there is a weak discrimination of the QLS film of **1** and **2** to the different concentrations of NO₂ (800, 400 to 200 ppm) in N₂. A similar response was also observed when the sensor operates in ambient air. The time-dependent current plots of the QLS films of **1** and **2** exposed to different concentrations of NO₂ from 800, 400 to 200 ppm in ambient air are shown in Fig. S3 in the ESI.† Apart from drying the air, no further precautions were taken, showing that the fabricated sensor is selective for NO₂.⁴²

3 Conclusion

In summary, two novel amphiphilic porphyrin zinc compounds with different hydrophilic polyoxyethylene substituents, [ZnT(OC₂H₄OC₂H₄OH)PP] (**1**) and [ZnT(OC₂H₄NN15C5)PP] (**2**), were designed, synthesized and fabricated into the QLS films to detect the NO₂ gas sensor properties at room temperature. UV-vis, XRD and AFM results suggest that the stronger intermolecular interaction with the π - π stacking interaction between tetrapyrrole rings in the porphyrin molecules of **1** compared to **2** leads to increased molecular packing and improved film-crystallinity. Correlatively, the conductivity of the QLS film of **1** is more than 1 order of magnitude higher than that of **2**. The more sensitive, stable and reproducible responses to NO₂ gas at concentrations 200 and 800 ppm are obtained for the film of **1** in a faster response/recovery cycle of only 4/6 min. Unexpectedly, a decreased current response towards NO₂ for the QLS films of both **1** and **2** was obtained for the first time, which unambiguously demonstrated the n-type semiconducting nature of **1** and **2**.

4 Experimental

4.1 Chemicals

All solvents were dried and distilled according to standard procedures. All other solvents and reagents such as Zn(OAc)₂·2H₂O were used as received. All air-sensitive reactions were carried out under a nitrogen atmosphere. DMF and dichloromethane were freshly distilled just before use. Column chromatography was carried out on silica gel (Merck, Kieselgel 60, 200–300 mesh) with the indicated eluent. The 5-(benzo-(4-(2-(2-hydroxyethoxy)ethoxy))-10,15,20-triphenylporphyrinato zinc complex [ZnT(OC₂H₄OC₂H₄OH)PP] (**1**) and the 5-(4-(2-(4,10-*N*,*N*-15-crown-5)ethoxy))-10,15,20-triphenylporphyrinato zinc complex [ZnT(OC₂H₄NN15C5)PP] (**2**) were synthesized and purified according to published procedures.²⁰ The detailed synthesis procedures together with the structural characterization are described in the ESI.†

4.2 Fabrication of the thin films

Thin films for device applications were fabricated as follows: (i) quasi-Langmuir–Shäfer (QLS) film of [ZnT(OC₂H₄OC₂H₄OH)PP] (**1**): firstly, 5.0 mL of chloroform solution of [ZnT(OC₂H₄OC₂H₄OH)PP]

(1) ($\sim 1 \times 10^{-6} \text{ mol L}^{-1}$) was put into a cylindrical glass container (diameter: 9.5 cm, height: 1.5 cm, volume: 106.3 cm³), then 65 mL of water was slowly added into the container. (**Caution:** the amount of water added cannot cover completely the surface of the chloroform solution so as to keep the path for the evaporation of the solvent, CHCl₃.) During the solvent evaporation, the molecules gradually assembled to form some fine membrane structures at the CHCl₃/water interface and in turn the densely packed film on the water surface until complete evaporation of CHCl₃. The film can be easily transferred from the water surface onto the ITO substrate by horizontal lifting, *i.e.* the slide was horizontally and carefully lowered onto the film surface and then raised.²⁰ This process was repeated to obtain the required number of layers. Residual water on the substrate, between transfer steps and after the final transfer, was removed with a stream of N₂. (ii) Quasi-Langmuir–Shäfer (QLS) film of [ZnT(OC₂H₄NN15C5)PP] (2): it was fabricated according to QLS technology described above.²⁵

4.3 Electrical experiments and measurements of the NO₂ gas sensor

The fundamental electrical measurements were performed using a Hewlett–Packard (HP) 4140B parameter analyzer at room temperature. Current–voltage (*I–V*) curves were registered in the –100 to 100 V voltage range with 5 V increments, starting and finishing at 0 V bias to avoid irreversible polarization effects. All experiments were conducted at least twice to ensure reproducibility. The interdigitated electrode array is composed of 10 pairs of ITO electrode digits deposited onto a glass substrate with the following dimensions: 125 μm electrode width, 75 μm spacing, 5850 μm overlapping length and 20 nm electrode thickness. Conductivity, σ can be calculated by eqn (1),

$$\sigma = \frac{d \times I}{(2n - 1) \times L \times h \times V} \quad (1)$$

where *d* is the interelectrode spacing, *I* the current, *n* the number of electrode digits, *L* the overlapping length of the electrodes, and *h* the film thickness if it is less than that of the electrodes or the electrode thickness when the film thickness exceeds that of the ITO electrodes. The NO₂-sensing properties of samples were examined by exposing the corresponding films to different concentrations of NO₂ gas and measuring the current changes of the films at a constantly polarized voltage of 9 V.

Acknowledgements

This work was financially supported by the National Natural Science Foundation of China (No. 21371073), Research Foundation from China University of Petroleum (East China) (Y1510051) and Shandong Academy of Agricultural Sciences Cooperation Guiding Plan Project (Grant No. 2014YDZH04).

Notes and references

- 1 F. Souza and O. Ito, *Chem. Soc. Rev.*, 2012, **41**, 86.
- 2 D. Gust, T. Moore and A. Moore, *Acc. Chem. Res.*, 2009, **42**, 1890.

- 3 E. Mal'tsev, M. Brusentseva, V. Rumyantseva, D. Lypenko, V. Berendyaev, A. Mironov, S. Novikov and A. Vannikov, *Polym. Sci., Ser. A*, 2006, **48**, 146.
- 4 P. K. B. Palomaki, M. R. Civic and P. H. Dinolfo, *ACS Appl. Mater. Interfaces*, 2013, **5**, 7604.
- 5 V. Montes, C. Pérez-Bolívar, N. Agarwal, J. Shinar and P. Anzenbacher, *J. Am. Chem. Soc.*, 2006, **128**, 12436.
- 6 M. Seol, S. Choi, C. Kim, D. Moon and Y. Choi, *ACS Nano*, 2012, **6**, 183.
- 7 S. Rao, N. Naga Srinivas, D. Rao, L. Giribabu, B. Maiya, R. Philip and G. Kumar, *Opt. Commun.*, 2001, **192**, 123.
- 8 F. Pavinatto, A. Gameiro Jr, A. Hidalgo, L. Dinelli, L. Romualdo, A. Batista, N. Barbosa Neto, M. Ferreira and O. Oliveira Jr, *Appl. Surf. Sci.*, 2008, **254**, 5946.
- 9 P. Ma, Y. Chen, Y. Bian and J. Jiang, *Langmuir*, 2010, **26**, 3678.
- 10 X. Gong, T. Milic, C. Xu, J. Batteas and C. Drain, *J. Am. Chem. Soc.*, 2002, **124**, 14290.
- 11 G. Giancane and L. Valli, *Adv. Colloid Interface Sci.*, 2012, **17–35**, 171.
- 12 J. Pedrosa, C. Dooling, T. Richardson, R. Hyde, C. Hunter, M. Martín and L. Camacho, *Mater. Sci. Eng., C*, 2002, **22**, 433.
- 13 K. Garg, A. Singh, C. Majumder, S. Nayak, D. Aswal, S. Gupta and S. Chattopadhyay, *Org. Electron.*, 2013, **14**, 1189.
- 14 A. Dunbar, T. Richardson, J. Hutchinson and C. Hunter, *Sens. Actuators, B*, 2008, **128**, 468.
- 15 A. D'Amicoa, C. Natalea, R. Paolesseb, A. Macagnanoa and A. Mantinia, *Sens. Actuators, B*, 2000, **65**, 209.
- 16 S. Kladsomboon and T. Kerdcharoen, *Anal. Chim. Acta*, 2012, **757**, 75.
- 17 Y. Chen, M. Bouvet, T. Sizun, Y. Gao, C. Plassard, E. Lesniewska and J. Jiang, *Phys. Chem. Chem. Phys.*, 2010, **12**, 12851.
- 18 J. Gao, G. Lu, J. Kan, Y. Chen and M. Bouvet, *Sens. Actuators, B*, 2012, **166–167**, 500.
- 19 Y. Chen, M. Bouvet, T. Sizun, G. Barochi, J. Rossignol and E. Lesniewska, *Sens. Actuators, B*, 2011, **155**, 165.
- 20 G. Lu, Y. Chen, Y. Zhang, M. Bao, Y. Bian, X. Li and J. Jiang, *J. Am. Chem. Soc.*, 2008, **130**, 11623.
- 21 D. Li, H. Wang, J. Kan, W. Lu, Y. Chen and J. Jiang, *Org. Electron.*, 2013, **14**, 2582.
- 22 G. Lu, X. Zhang, X. Cai and J. Jiang, *J. Mater. Chem.*, 2009, **19**, 2417.
- 23 A. Satake and Y. Kobuke, *Org. Biomol. Chem.*, 2007, **5**, 1679.
- 24 M. Kasha, H. Rawls and M. El-Bayoumi, *Pure Appl. Chem.*, 1965, **11**, 371.
- 25 Y. Chen, M. Bouvet, T. Sizun, G. Barochi, J. Rossignol and E. Lesniewska, *Sens. Actuators, B*, 2011, **155**, 165.
- 26 (a) M. Yoneyama, M. Sugi, M. Saito, K. Ikegami, S. Kuroda and S. Iizima, *Jpn. J. Appl. Phys.*, 1986, **25**, 961; (b) J. Bourgoïn, F. Doublet, S. Palacin and M. Vandevyver, *Langmuir*, 1996, **12**, 6473; (c) H. Xiang, K. Tanaka, A. Takahara and T. Kajiyama, *Langmuir*, 2002, **18**, 2223.
- 27 H. Katz and Z. Bao, *J. Phys. Chem. B*, 2000, **104**, 671.
- 28 N. An, Y. Shi, J. Feng, D. Li, J. Gao, Y. Chen and X. Li, *Org. Electron.*, 2013, **14**, 1197.

- 29 J. Hill, W. Jin, A. Kosaka, T. Fukushima, H. Ichihara, T. Shimomura, K. Ito, T. Hashizume, N. Ishii and T. Aida, *Science*, 2004, **304**, 1481.
- 30 Y. Yamamoto, T. Fukushima, Y. Suna, N. Ishii, A. Saeki, S. Seki, S. Tagawa, M. Taniguchi, T. Kawai and T. Aida, *Science*, 2006, **14**, 1761.
- 31 Y. Gao, X. Zhang, C. Ma, X. Li and J. Jiang, *J. Am. Chem. Soc.*, 2008, **130**, 17044.
- 32 P. Ma, Z. Bai, Y. Gao, Q. Wang, J. Kan, Y. Bian and J. Jiang, *Soft Matter*, 2011, **7**, 3417.
- 33 (a) J. Liu, K. Yang and Z. Lu, *J. Am. Chem. Soc.*, 1997, **119**, 11061; (b) T. Yamamoto, H. Kokubo, M. Kobubo, M. Kobashi and Y. Sakai, *Chem. Mater.*, 2004, **16**, 4616.
- 34 M. Kimura, T. Muto, H. Takimoto, K. Wada, K. Ohta, K. Hanabusa, H. Shirai and K. Nagao, *Langmuir*, 2000, **16**, 2078.
- 35 Y. Che, A. Datar, X. Yang, T. Naddo, J. Zhao and L. Zang, *J. Am. Chem. Soc.*, 2007, **129**, 6354–6355.
- 36 Y. Chen, Y. Feng, J. Gao and M. Bouvet, *J. Colloid Interface Sci.*, 2012, **368**, 387.
- 37 T. Sizun, M. Bouvet, Y. Chen, J. Suisse, G. Barochi and J. Rossignol, *Sens. Actuators, B*, 2011, **159**, 163.
- 38 Y. Chen, D. Li, N. Yuan, J. Gao, R. Gu, G. Lu and M. Bouvet, *J. Mater. Chem.*, 2012, **22**, 22142.
- 39 P. Checcoli, G. Conte, S. Salvatori, R. Paolesse, A. Bolognesi, M. Berliocchi, F. Brunetti, A. D'Amico, A. Carlo and P. Lugli, *Synth. Met.*, 2003, **138**, 261.
- 40 F. Bohrer, A. Sharoni, C. Colesniuc, J. Park, I. Schuller, A. Kummel and W. Trogler, *J. Am. Chem. Soc.*, 2007, **129**, 5640.
- 41 H. Yan, P. Lee, N. Armstrong, A. Graham, G. Evmenenko, P. Dutta and T. Marks, *J. Am. Chem. Soc.*, 2005, **127**, 3172.
- 42 A. Andringa, C. Piliago, I. Katsouras, P. Blom and D. Leeuw, *Chem. Mater.*, 2014, **26**, 773.